Mechanisms of Specific and Nonspecific Binding of Architectural Proteins in Prokaryotic Gene Regulation†

James M. Benevides, Jessica Danahy, Jessica Kawakami, and George J. Thomas, Jr.*

School of Biological Sciences, University of Missouri—Kansas City, 5100 Rockhill Road, Kansas City, Missouri 64110-2499

Received May 16, 2007; Revised Manuscript Received January 4, 2008

ABSTRACT: IHF and HU are small basic proteins of eubacteria that bind as homodimers to double-stranded DNA and bend the duplex to promote architectures required for gene regulation. These architectural proteins share a common α/β fold but exhibit different nucleic acid binding surfaces and distinct functional roles. With respect to DNA-binding specificity, for example, IHF is sequence specific, while HU is not. We have employed Raman difference spectroscopy and gel mobility assays to characterize the molecular mechanisms underlying such differences in DNA recognition. Parallel studies of solution complexes of IHF and HU with the same DNA nonadecamer (5′ → 3′ sequence: TCTAAGTAGTTGATTCATA, where the phage λ H1 consensus sequence of IHF is underlined) show the following. (i) The structure of the targeted DNA site is altered much more dramatically by IHF than by HU binding. (ii) In the IHF complex, the structural perturbations encompass both the sugar–phosphate backbone and the bases of the consensus sequence, whereas only the DNA backbone is altered by HU binding. (iii) In the presence of excess protein, complexes of order higher than 1 dimer per duplex are detected for HU:DNA, though not for IHF:DNA. The results differentiate structural motifs of IHF:DNA and HU:DNA solution complexes, provide Raman signatures of prokaryotic sequence-specific and nonspecific recognition, and suggest that the architectural role of HU may involve the capability to recruit additional binding partners to even relatively short DNA sequences.

IHF[1] and HU are small basic proteins of eubacteria that play important roles in nucleoid organization and gene regulation (*1–5*). Both proteins bind as dimers to duplex DNA, introduce significant bending of the double helix, and facilitate the formation of higher order nucleoprotein complexes. A more detailed examination of their architectural and functional properties has been given (*6*). The IHF and HU subunits share 30–40% sequence identity, depending upon species, and exhibit a common fold (α-helical core with protruding β-ribbon arms that wrap around DNA) (*7–11*). Nevertheless, these architectural proteins exhibit distinct binding preferences. HU binds DNA nonspecifically and with relatively low affinity ($K_d \sim$ 200–2500 nM) (*10*), although significantly enhanced binding has been noted for DNA sites that contain nicks (*12*), four-way junctions (*13*), or other structural anomalies (*14, 15*). Conversely, IHF binds DNA specifically and with much higher affinity ($K_d \sim$ 2–20 nM) at sites containing the consensus sequence WATCARXXXXT-TR (W is either A or T; R is either A or G; X is any DNA base) (*16*). Nonspecific and very low affinity binding has also been reported for IHF ($K_d \sim$ 20–30 μM) (*6*).

Biochemical and biophysical studies confirm that IHF and HU also differ substantially in their DNA-binding cooperativities and in the structural outcomes of binding. The available data consistently support noncooperative DNA binding for IHF and provide evidence of a helix bend angle of ~160° (*7, 17, 18*). In the case of HU, on the other hand, both low and high cooperativities of DNA binding, as well as moderate (70°) and large (140°) helix bend angles, have been reported, depending upon the particular DNA target (*19–22*). Recent analyses suggest a direct correlation between the magnitude of the HU-induced DNA bend angle and the length or topology of the DNA target, possibly reflecting additional contacts between HU and DNA in targets of greater length (*6*) or topological diversity (*23*). Solution results suggest that HU may function to stabilize already bent DNA, while IHF induces bending in otherwise unbent DNA sequences (*23*).

To further characterize the DNA recognition mechanisms of these architectural proteins, we have employed Raman difference spectroscopy as a means of comparing solution structures of IHF and HU complexes with the same DNA sequence. In this analysis we have employed a nonadecameric DNA target, TCTAAGTAGTTGATTCATA, which incorporates the phage λ H1 consensus sequence of IHF (underlined). The results demonstrate dramatic differences in the structural perturbations induced by IHF and HU in a common DNA substrate. Significant among these are distinctive modes of electrostatic interaction between DNA phos-

† Paper LXXXVI in the series Raman Spectral Studies of Nucleic Acids. Supported by National Institutes of Health Grant GM54378.

* To whom correspondence should be addressed. E-mail: thomasgj@umkc.edu. Telephone: 816-235-5247. Fax: 816-235-1503.

[1] Abbreviations: HUBst, HU protein from *Bacillus stearothermophilus*; IHF, integration host factor from *Escherichia coli*; HMG, high mobility group; HEPES, *N*-(2-hydroxyethyl)piperazine-*N*′-2-ethanesulfonic acid; EtBr, ethidium bromide; HPLC, high-pressure liquid chromatography; EMSA, electrophoretic mobility shift assay; FRET, fluorescence resonance energy transfer; UVRR, ultraviolet resonance Raman spectroscopy; bp, base pair.

10.1021/bi7009426 CCC: $40.75
Published on Web 02/27/2008

phates and basic side chains of the architectural proteins (*24–26*). The results are discussed in relation to the available crystal structures of IHF:DNA and HU:DNA complexes and compared with previously reported solution Raman studies of complexes of HU with linear and circular forms of 222-bp DNA (*23*). We also show that the Raman spectroscopic signatures of IHF:DNA and HU:DNA recognition support and extend the profiles proposed previously as diagnostic of specific and nonspecific recognition, respectively (*22, 27, 28*).

MATERIALS AND METHODS

Expression and Purification of HUBst. HU protein from *Bacillus stearothermophilus* (HUBst) was overexpressed in *Escherichia coli* BL21(DE3)pLysS cells and purified as previously described (*29, 30*). HUBst concentrations were determined by measurement of UV absorbance at 258 nm (ϵ_{258} = 0.076 mL·mg^{-1} cm^{-1} = 1482 M^{-1} cm^{-1}) using a Cary 3E spectrophotometer (Varian, Inc., Palo Alto, CA) and assuming a subunit molecular mass of 9716 Da (*29, 31*).

Expression and Purification of IHF. Integration host factor (IHF) from *E. coli* was overexpressed in *E. coli* BL21(DE3)pLysS cells and purified as previously described (*7*) with the following modifications: 0.5 mL of glucose solution (0.2 g/mL) was added to the LB media and LB plates used in the expression procedure; the concentration of glycerol in heparin and cation-exchange buffers was reduced to 10%. IHF concentrations were determined by UV absorbance measurements at 276 nm (ϵ_{276} = 5800 M^{-1} cm^{-1}) using a Cary 3E spectrophotometer (Varian, Inc., Palo Alto, CA). The final purified protein was dialyzed against 50 mM ammonium bicarbonate, lyophilized, and stored at −80 °C.

Oligonucleotide Purification and Characterization. HPLC-purified 5′ → 3′ oligonucleotides TCTAAGTAGTTGATTCATA and TATGAATCAACTACTTAGA were purchased from Sigma Genosys, The Woodlands, TX. Solutions of the two strands (each at ∼1 mg/mL) were mixed in equimolar amount on the basis of microgram/OD_{260} values supplied by the vendor, and the mixture was annealed by heating in a dry bath to 80 °C for 30 min followed by slow cooling to room temperature. Size exclusion chromatography (SEC) on a Superdex 75 10/300 GL Tricorn high-performance column (Amersham Biosciences, Piscataway, NJ) revealed that only the duplex was present.

Electrophoresis. IHF and HUBst stock solutions were prepared in EMSA binding buffer (10 mM Tris, 1 mM EDTA, 100 mM NaCl). Each reaction mixture (nonadecamer and either HUBst or IHF) was incubated at room temperature for 20 min to promote binding. Three microliters of 6× EMSA gel loading solution (Molecular Probes, Eugene, OR) was then added. Samples were loaded onto 4–20% TBE gradient gels (Lonza, Rockland, ME) that had been prerun at 140 V for 30 min at 4 °C. The DNA concentration in each gel lane was held constant at 0.4 μM, while the protein concentration among lanes varied from 0.2 to 3.2 μM for HUBst and from 0.2 to 1.2 μM for IHF. After being loaded, gels were run for 90 min at 150 V and 4 °C. Gels were stained with a solution of SYBR green (Molecular Probes, Eugene, OR) for 20 min. After being rinsed with deionized water, the gels were scanned on a Typhoon 9400 imager (Amersham Biosciences, Piscataway, NJ).

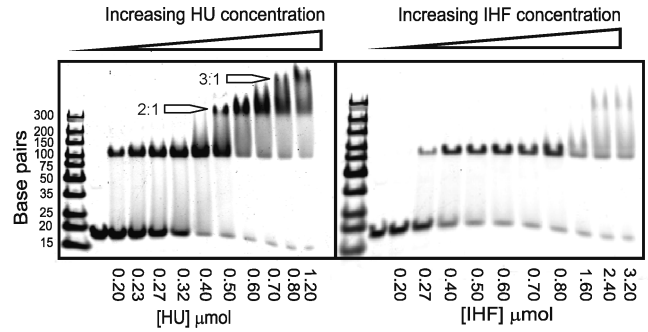

FIGURE 1: EMSA gels of complexes formed by HU (left) and IHF (right) with the 19-bp DNA target sequence (see text). DNA concentration is 0.4 μM in each lane. In both panels lane 1 contains DNA standards (15–300 bp) and lane 2 contains protein-free 19-bp DNA. HUBst and IHF concentrations (μM) are indicated along the bottom axis. In the left panel positions of the 1:2 and 1:3 HUBst:DNA complexes are indicated.

Raman Spectroscopy. Complexes of specific stoichiometries were prepared using the known molar extinction coefficients of DNA (annealed duplex, as prepared above), HUBst (ϵ_{258} = 1482 M^{-1} cm^{-1}), and IHF (ϵ_{276} = 5800 M^{-1} cm^{-1}). Each was prepared by dissolving the appropriate weight of lyophilized DNA in the protein solution. Aliquots (∼8 μL) were sealed in glass capillaries (KIMAX No. 34500), mounted in the sample illuminator of the Raman spectrophotometer, and thermostated at 15 °C for collection of spectra.

Raman spectra were collected on a Kaiser Optical HoloSpec VPT spectrometer (Ann Arbor, MI) equipped with a liquid nitrogen cooled, charge-coupled device detector optimized for the near-infrared region (model 1024EHRB; Roper, Trenton, NJ). Spectra were excited at 752 nm with ∼150 mW of radiant power from a titanium:sapphire laser (model 890; Coherent, Palo Alto, CA), which was pumped at 532 nm (model Millennia X; Spectra-Physics, Mountain View, CA). Each spectrum shown is the average of 20 or more exposures of 200 s each. Raman wavenumbers were calibrated using the emission lines from a neon lamp and the 459 cm^{-1} band of liquid CCl_4. Weak scattering by the aqueous solvent was removed using established computer subtraction techniques (*32*). Raman markers of the DNA phosphate group (1092 cm^{-1}) and the protein phenylalanine ring (1001 cm^{-1}) were employed for spectral intensity normalizations, as also described previously (*33*). Raman difference peaks and troughs representing at least 5% of the parent band intensity and with a signal-to-noise ratio of at least 2:1 were judged to be experimentally significant.

RESULTS AND INTERPRETATION

Electrophoretic Characterization of HUBst:DNA and IHF:DNA Complexes. HUBst and IHF binding to nonadecameric DNA was investigated by EMSA (Figure 1) at constant concentration of DNA (0.40 μM) and increasing concentration of protein dimer (0.2–3.8 μM for HUBst and 0.2–1.2 μM for IHF). The gel data yield K_d values of 0.33 ± 0.07 and 0.28 ± 0.5 μM, respectively, for HUBst and IHF. Figure 1 establishes that both HUBst and IHF bind the 19-mer and form well-defined 1:1 complexes. As protein concentrations are increased, HUBst forms two additional stable complexes (Figure 1, left), while IHF forms a single less stable complex (Figure 1, right, lanes 10–12) that appears to rapidly

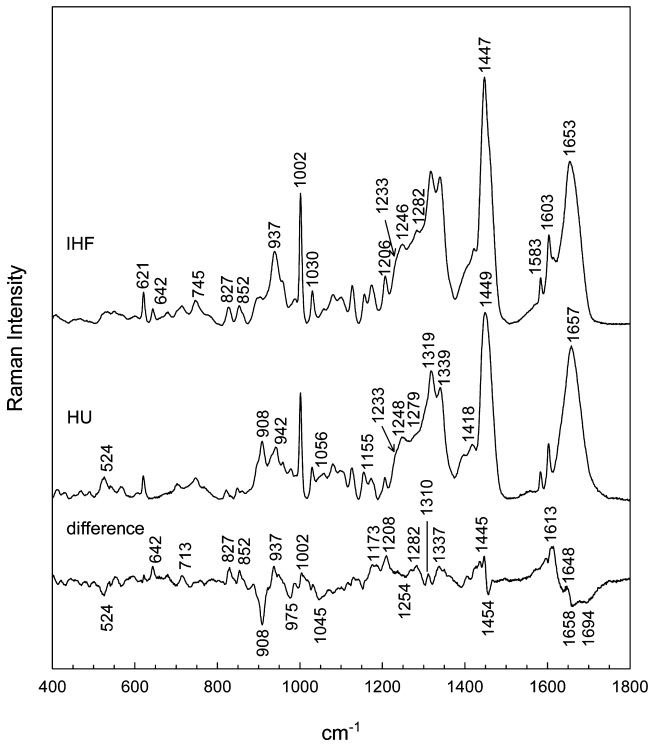

FIGURE 2: Raman spectra (400–1800 cm^{-1}; 752 nm excitation) of solutions of IHF (top) and HUBst (middle) at 20 $\mu g/\mu L$ in 10 mM Tris (pH 7.5) + 100 mM NaCl and their computed difference spectrum (bottom).

Table 1: Solution Secondary Structures of IHF and HUBst Based upon Curve Fitting of Raman Amide I Bands[a]

structure type	HUBst	IHF
α-helix	42 ± 2% (47%)[b]	47 ± 2% (40%)[c]
β-strand	24 ± 3% (24%)	25 ± 3% (29%)
irregular	34 ± 3% (29%)	28 ± 3% (31%)

[a] Method of Berjot (*34*). [b] Values in parentheses are based upon the X-ray crystal structure of HUBst (*9*). The X-ray values are derived from 80 residues and not the 90-residue monomer employed in the Raman analysis. [c] Values in parentheses are based upon the X-ray structure of the IHF cocrystal (*7*).

dissociate. This second IHF complex may reflect nonspecific binding of the protein to the initially formed specific complex.

Comparison of HUBst and IHF Secondary Structures. Raman spectra of IHF and HUBst excited at 752 nm are presented in Figure 2. The Raman signature of HUBst (middle trace) corresponds closely to that obtained previously using 532 nm excitation (*30*). Both IHF and HUBst exhibit an intense amide I band centered near 1655 cm^{-1} and a complex amide III profile (peaks near 1233, 1250, 1280, and 1310 cm^{-1}) indicating similar folds. Quantitative estimates of secondary structure types from Raman amide I band analysis (*34*) and comparison with results from X-ray crystal studies (*7, 9*) are given in Table 1. The Raman amide I analysis reveals slightly more α-helix in IHF (47 ± 2%) than in HUBst (42 ± 2%) and a correspondingly reduced amount of irregular structure. This is also apparent in the Raman difference spectrum (Figure 2, bottom trace), which shows for IHF greater intensity of α-helix markers (937, 1282, 1310, and 1648 cm^{-1}) and lower intensity of markers diagnostic of irregular structure (1254 and 1658 cm^{-1}) and turn (1694 cm^{-1}). The β-strand content is comparable for both proteins.

Table 2: Raman Frequencies and Assignments of HUBst and IHF

Raman wavenumber[a]		
HUBst	IHF	assignments[b]
524	529	F, α-helix
541	550	V
567	567	amide VI
605	601	L
621	621	F
	642	Y
	679	H
703	703	M
	715	H
747	745	I, L, K
768		?
	778	Y
822		F
	827	Y
850		?
	852	Y
860	860s	V, L
908	904	A
943	937	K, V, L; α-helix [C^{α}–C^{β} stretch]
959	957s	K, L
979		?
	988	H, I
1002	1003	F
1030	1030	F
1058	1059	K, R, Q, N [C−N stretch]
1081	1080	[C−C stretch]; K, R, Q, N [C−N stretch]
1100	1100	[C−C stretch]
1127	1128	[C−C stretch]
1156	1156	I, V, [CH_3 deformation]
1174	1174	Y, F; [CH_3 deformation]
1207	1208	F, Y
1238s	1233s	amide III (β-strand)
1250	1246	amide III (irregular structure)
1279s	1282	amide III (α-helix)
1308s		amide III (α-helix)
1320	1318	[CH_2 deformation]
1342	1340	[$C^{\alpha}H$ deformation], [C^{α}−C stretch]
1398s	1408	[COO^- stretch]
1420	1422	Q; [CH_2 deformation]
1450	1447	[CH_2 deformation]
	1457	[CH_3 deformation]
1584	1583	F
1603	1603	F
	1614	Y
	1653	amide I (α-helix)
1658		amide I (α-helix, irregular structure)

[a] In cm^{-1} units from data of Figure 2; s denotes shoulder to a more intense band. [b] Assignments to specific amino acid side chains (one letter abbreviations) are from refs (*57–59*). Brackets ([ ]) indicate chemical group frequencies common to more than one type of side chain.

The remaining difference features in the bottom trace of Figure 2 reflect the different primary structures of the two proteins. Assignments to specific protein side chains are given in Table 2.

Raman Signature of 19-bp DNA. The Raman spectrum of the DNA nonadecamer duplex employed as the binding target for both HUBst and IHF is shown in Figure 3. Raman markers (*35*) of the *gauche*$^-$ (g^-) conformations of the deoxyribosylphosphate backbone torsion angles α and ζ at 789 and 834 cm^{-1} and of the C2′-*endo/anti* deoxynucleoside conformations at 669 (dT), 681 (dG), and 728 cm^{-1} (dA) identify the duplex as *B* DNA. The greater intensity of bands of dA and dT relative to those of dG and dC is consistent with the ~3:1 ratio of AT to GC base pairs in the duplex.

Raman Analysis of the 1:1 HUBst:DNA Complex. The Raman spectrum of the 1:1 complex of HUBst and the

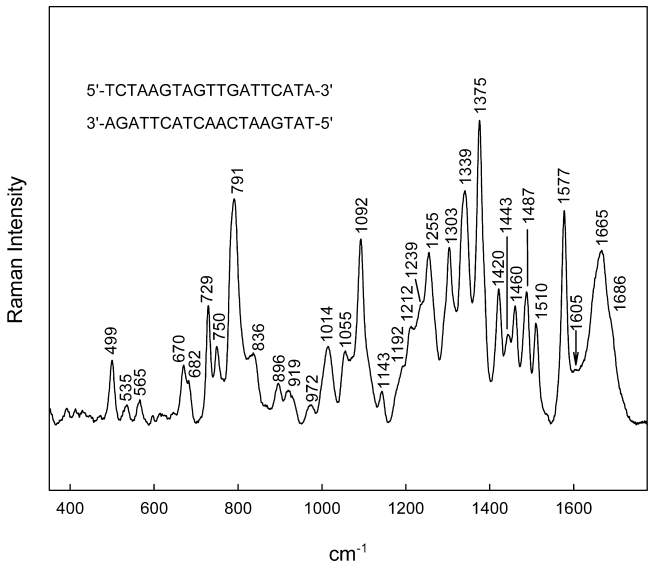

FIGURE 3: Raman spectrum of the 19-bp DNA target sequence at 25 μg/μL in 10 mM Tris (pH 7.5) + 100 mM NaCl.

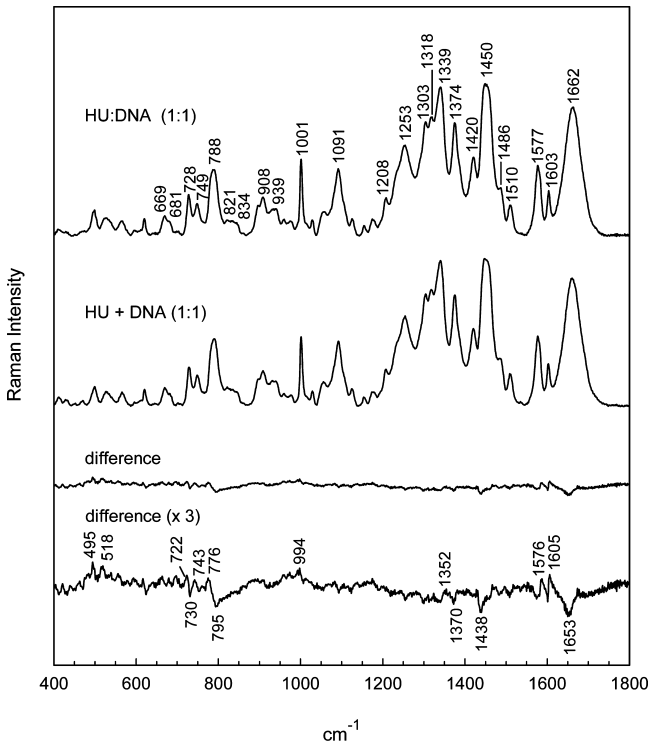

FIGURE 4: Raman spectrum of the 1:1 HUBst:DNA complex (top), the spectral sum of constituents (middle), the computed difference spectrum (second from bottom), and a 3-fold amplification of the difference spectrum (bottom). Although both DNA and HUBst are expected to contribute intensity at 1605 cm^{-1} (Figures 2 and 3), we assign the observed difference peak at 1605 cm^{-1} primarily to DNA rather than HUBst, owing to the documented structure-sensitive Raman marker of DNA at this position (*60*). The putative HUBst contribution, which is due to phenylalanine, is not conformation sensitive (*57*).

nonadecamer is compared with the spectral sum of constituents in Figure 4. The amplified difference spectrum (Figure 4, bottom trace) exhibits numerous peaks and troughs consistent with modest conformational rearrangement of the DNA target upon HUBst binding. [We note that, as expected, the *relative* intensities of difference features here are distinct from those observed with shorter wavelength laser excitation, i.e., 532 nm (*22*). This is particularly evident when comparing bands of the 1200–1500 and 750–1100 cm^{-1} regions, which are due respectively to base and sugar–phosphate modes. This is consistent with the fact that the latter do not benefit greatly from preresonance intensity enhancements when 752 nm excitation is employed.]

The prominent peak/trough features in the interval 770–850 cm^{-1} of the bottom trace of Figure 4 show that the conformation of the backbone C5′−O5′P−O3′−C3′ network is significantly perturbed by HUBst. The spectral changes are consistent with a localized rearrangement to a conformation differing from canonical *B* DNA. On the basis of the diminished intensity of Raman markers of *B* DNA (795–840 cm^{-1}), we estimate that 4 ± 1 of the 38 nucleotides are affected. Because the C5′H_2 group of deoxyribose is the source of the Raman band near 1438 cm^{-1} (*31*), the difference trough at this wavenumber value is interpreted as evidence of a conformational change specifically involving six or more of the C5′H_2 groups. Additional perturbations to DNA structure are indicated by the difference bands of DNA bases at 1370, 1575, and 1605 cm^{-1}. The latter two are assigned to purines and may reflect altered base hydrogen-bonding environments in the complex. The trough at 1653 cm^{-1} in the Figure 4 difference spectrum is the only feature that can be attributed to the protein component of the complex, namely, the amide I band for the α-helix. It reflects a small (∼5%) reduction in HUBst α-helicity with complex formation.

Raman Analysis of the 1:1 IHF:DNA Complex. The Raman spectrum of the 1:1 complex of IHF and the nonadecamer is compared with its spectral sum of constituents in Figure 5. The distribution of intense peaks and troughs over the entire difference spectrum (bottom trace of Figure 5) demonstrates that the structure of the DNA target is altered much more by IHF than by HUBst (cf. Figure 4). Comparison of Figures 4 and 5 also demonstrates the uniqueness of the respective Raman difference signatures for these two complexes. The results on IHF:DNA are interpreted as follows.

(A) Conformation and Environment of the DNA Backbone. The difference peaks at 777 and 807 cm^{-1} (Figure 5, bottom) are consistent with a localized conformational change in the DNA phosphodiester backbone, which is qualitatively similar to the spectral changes observed for the *B*-to-*A* transitions of DNA and poly(dA-dT)·poly(dA-dT) (*37–39*). The difference peak intensities indicate that only 6 ± 1 of the 36 nucleotide phosphates are affected. We emphasize that a *B*-to-*A* transition is not being proposed for the complex (see below); rather, we interpret these spectral differences as evidence of a change only in the local geometry of approximately six phosphodiester linkages (*40*). Additionally, the Raman phosphodioxy marker centered near 1095 cm^{-1} is broadened by complex formation, indicating a change in the local electrostatic environment of several DNA phosphate groups. This spectral change, which is not observed for HUBst:DNA (cf. Figures 4 and 5), appears to be specific to IHF:DNA.

(B) Conformation and Environment of the Deoxynucleosides. Informative Raman markers of the deoxynucleoside moieties include several that are diagnostic of sugar conformation (600–780 cm^{-1}) and several that are responsive to changes in interbase stacking and hydrogen-bonding

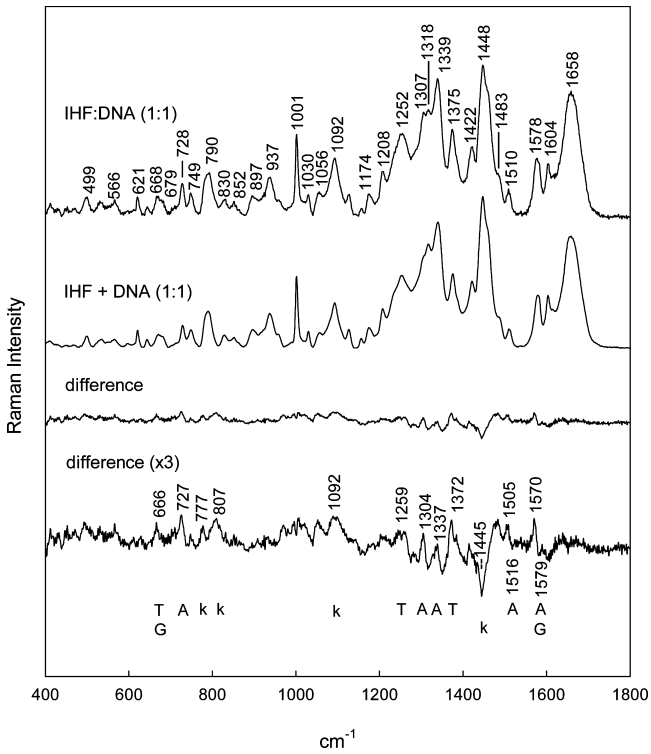

FIGURE 5: Raman spectrum of the 1:1 IHF:DNA complex (top), the spectral sum of constituents (middle), the computed difference spectrum (second from bottom), and a 3-fold amplification of the difference spectrum (bottom). Raman band assignments to DNA bases (A, C, G, T) and backbone (k) are indicated along the abscissa.

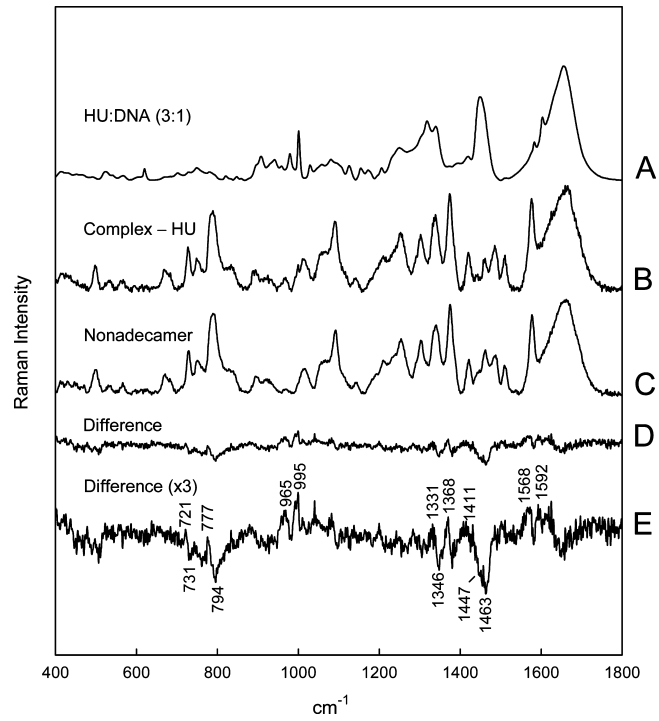

FIGURE 6: (A) Raman spectrum of the 3:1 HUBst:DNA complex. (B) Raman signature of DNA that is perturbed by HUBst binding in (A), which is generated by subtracting the spectrum of free HUBst from that of the complex. (C) Raman spectrum of DNA (from Figure 3). (D) Raman signature of HUBst that is perturbed by DNA binding in (A), which is generated by subtracting the spectrum of free DNA from (B). (E) 3-fold amplification of (D). [Comparison of (E) with the amplified difference spectra of Figures 4 and 5 is given in the text.]

interactions (1200–1600 cm^{-1}) (*41–44*). Virtually all of these bands are significantly affected by the global *B*-to-*A* transition of DNA (*36, 38, 39*), which involves changes in deoxyribosyl conformation (C2′-*endo* to the C3′-*endo*) and base orientations. Although the Raman signature of a global *B*-to-*A* transition is not observed for IHF binding to DNA, the Figure 5 difference spectrum (bottom trace) does reveal pronounced changes in many bands of the 600–780 and 1200–1600 cm^{-1} intervals. For example, the Raman markers of dA (727, 1259, 1304, 1337, 1505, and 1570 cm^{-1}) and dT (666, 1245, and 1372 cm^{-1}) undergo intensity increases with IHF binding, implying recovery of Raman hypochromism (i.e., base unstacking) upon complex formation. These intensity increases are about 50% of those observed for the unstacking (melting) of poly(dA-dT)·poly(dA-dT) (*39*), suggesting that about half of the 28 bases are unstacked by IHF. In addition to base unstacking, evidence of altered hydrogen-bonding interactions of base donor and acceptor groups (wavenumber shifts 1516 → 1505, 1579 → 1571) (*37, 40*) and a change in the average hydrophobic environment of thymine methyl groups (peak at 1372 cm^{-1}) (*27, 46*) also appear in the Figure 5 difference spectrum.

Finally, deoxyribosyl markers of the region 1415–1465 cm^{-1} (*36*) also contribute to the Figure 5 difference spectrum. These signal a change in the average environments of C2′ and C5′ methylene groups. The positions and intensities of these deoxyribosyl bands are particularly sensitive to changes in helix geometry (*40, 47–49*). In protein/DNA complexes where the DNA target is known to undergo significant distortion, such as bending, the intensities of these bands are also significantly affected (*22, 23, 27*). In the bottom trace of Figure 5, we find a prominent trough at 1445 cm^{-1}, which is consistent with a large distortion in helix geometry attendant with IHF binding. The observed trough is severalfold greater than the corresponding feature (1438 cm^{-1}) in the Figure 4 difference spectrum, which implies a much greater impact of IHF than HUBst on the local environment of deoxyribosyl groups.

Comparison of HUBst:DNA and IHF:DNA Complexes. As shown in Figure 1, the stepwise addition of HUBst to a fixed concentration of the nonadecamer leads to the formation of HUBst:DNA complexes of order greater than 1:1, including apparent 2:1 and 3:1 complexes (arrows). In the solution containing the 3:1 molar ratio of HUBst:DNA (Figure 1A, lane 12), all of the DNA is protein-bound and exists as a mixture of 2:1 and 3:1 complexes. For convenience, we refer to this as the 3:1 complex. The Raman spectrum of this 3:1 complex is shown in Figure 6A. Although the spectrum is dominated by bands of HUBst, the subtraction of the HUBst component (Figure 6B) reveals Raman bands of the protein-bound nonadecamer (Figure 6C). Subsequent subtraction of the spectrum of protein-free nonadecamer yields the difference signature of this 3:1 complex (Figure 6D; amplified 3-fold in Figure 6E).

Figure 7 shows that the 1:1 and 3:1 HUBst:DNA complexes exhibit similar difference profiles in a narrow spectral interval (700–800 cm^{-1}). Conversely, distinct difference profiles are observed in the remainder of the spectrum, including novel difference features (peaks at 1331, 1368, and 1411 cm^{-1} and troughs at 1346 and 1463 cm^{-1}) and enhanced intensities for the 3:1 complex. These signal enhanced perturbation of DNA structure in the 3:1 complex.

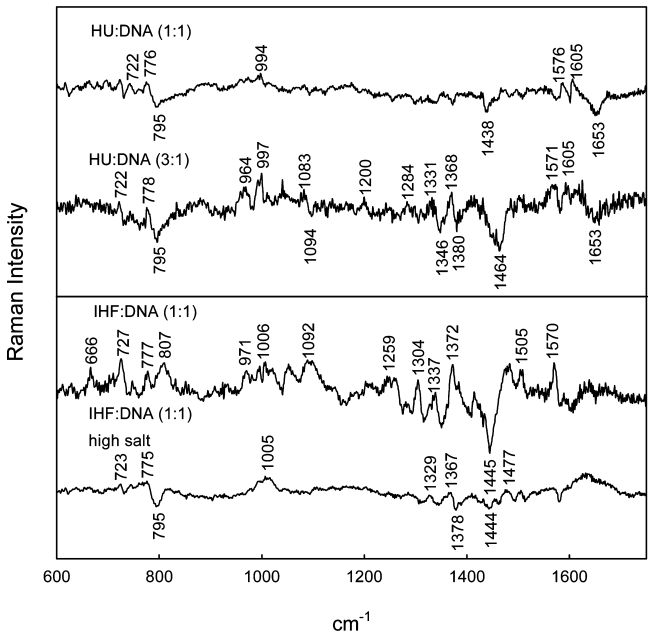

FIGURE 7: Comparison of normalized Raman difference profiles of the DNA complexes of HUBst (top) and IHF (bottom), as labeled.

The difference spectra of the 1:1 and 3:1 HUBst:DNA complexes (upper panel of Figure 7) are also compared with the 1:1 IHF:DNA complex in 100 and 250 mM NaCl (lower panel of Figure 7). EMSA gels (not shown) indicate that the 1:1 IHF:DNA complex, which is stable in 100 mM NaCl, becomes destabilized in 250 mM NaCl. The Raman difference spectrum shows that this leads to DNA perturbations closely resembling those of the nonspecific 1:1 HUBst:DNA complex (cf. top and bottom traces of Figure 7). The data are consistent with weak and nonspecific binding of IHF to its cognate DNA sequence in 250 mM NaCl.

DISCUSSION AND CONCLUSIONS

Crystal structure results show that the specific binding of IHF to its cognate sequence produces a robust distortion of the *B*-form structure including sharp bending of the double helix (160° bend angle) (*7*). The present results confirm this finding for the 1:1 IHF:DNA complex in 100 mM NaCl solution. We categorize the Raman difference signature of this IHF:DNA complex in physiological salt as that of *specific* protein binding, which leads to a large static bend in the DNA target. The more attenuated Raman difference signature observed here for the 1:1 HUBst:DNA complex in solution is interpreted as evidence of a marginally distorted DNA target. We identify this Raman signature as that of *nonspecific* protein binding which does not induce a large static bend in DNA. It should be noted that although no equivalent HUBst:DNA crystal structure is currently available for comparison with the Raman solution results, a crystal structure of *Anabaena* HU with DNA incorporating unpaired and mismatched bases shows significant static bending (74–91°) near the insertion site (*10*). However, it is not possible to quantify the extent to which the observed bending in the crystal structure is dependent upon mismatching and unpairing.

Figure 8 shows the distribution of basic protein side chains within hydrogen-bonding distances of DNA phosphates in both the IHF and HU crystal structures (*7, 10*). Hydrogen-bonding distances, which serve as a gauge of the proximity of basic side chains to DNA phosphates, are significantly different in the two crystal structures. The clusterings of IHF basic residues, represented by arrows at and adjoining the DNA consensus site (Figure 8A), do not occur for HU (Figure 8B). Because of the helix screw axis in the bent duplex, all of the arrow-marked IHF residues face the concave surface of the protein. The HU complex lacks this density of potential electrostatic interaction. This structural distinction is consistent with the observed differences in perturbation of Raman markers of the DNA phosphates. Although the *Anabaena* HU:DNA and HUBst:DNA structures are likely to differ in bending and other details, as noted above, their surface charge distributions are very similar (*9, 10*).

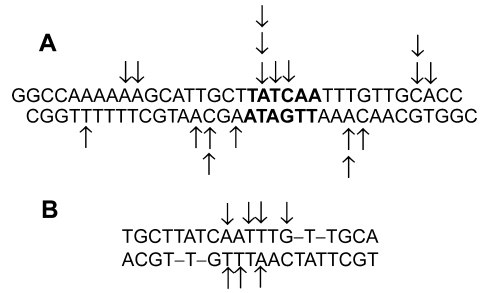

FIGURE 8: Diagram comparing the distributions of DNA sites (arrows) that have been shown by X-ray crystallography (*7*) (*10*) to interact via their nucleotide phosphates with basic side chains of the IHF (A) and HU (B) proteins.

The IHF-induced structural perturbations of DNA, which introduce *A*-form character to a significant population of backbone residues, may contribute to protein recognition required for *in vivo* IHF function. The possible role of induced *A*-form structure as a contributor to protein recognition (indirect readout) has been explored previously (*50*).

The more modest change in Raman conformation makers associated with HUBst binding to the nonadecamer is compatible with reduced helix distortion. Recently, we compared HUBst binding to a 222 base pair linear fragment and to its circularized counterpart. We showed that the circularized DNA target suffered more extensive structural reorganization than the linear form (*23*). We interpreted this as consistent with a role for HUBst in which the protein functions to opportunistically stabilize bent regions of DNA and to manipulate relatively flexible segments of DNA rather than to introduce curvature *de novo* in unbent or rigid DNA as is the case for IHF. The present results on the 1:1 complexes of the nonadecamer with IHF and HUBst are in accord with such an interpretation. In the present case, the combined Raman and EMSA data suggest that a stable complex forms with HUBst binding in which only modest perturbation (bending?) of the double helix ensues. The present results also are consistent with a recent ultraviolet resonance Raman (UVRR) study of the effects of HU binding to model oligonucleotides. Two oligonucleotides, which had been shown by fluorescence resonance energy transfer (FRET) to bend in response to HU binding (*20*), exhibit significant perturbations to their UVRR spectra with HU binding. In contrast, an oligonucleotide that exhibits little bending, as assessed by FRET, manifests less significant

Raman perturbations. This has been interpreted as evidence against significant DNA distortion (*51*).

Initial studies of the nonspecific binding of *E. coli* HU to duplex DNA suggested a binding site of 9 bp (*52, 53*). More recently, on the basis of analytical ultracentrifugation and fluorescence anisotropy measurements (*21*), it has been suggested that the number of base pairs comprising the binding site may vary as a function of overall DNA length. For example, a binding site of 6 bp was inferred in the case of a 13-bp DNA target (*21*). The present experiments (Figure 1) are consistent with this value and imply that up to three HUBst dimers can be accommodated by the 19-bp target employed here (Figure 1).

Recently, on the basis of stopped-flow fluorimetry, it has been proposed that IHF:DNA complex formation involves a two-step mechanism in which the initial step of rapid IHF binding is followed by DNA bending (*54*). In a subsequent series of combined stopped-flow and temperature-jump measurements it was determined that the DNA bending rate and activation energy are similar to the base pair opening rate and activation energy associated with opening a single A·T base pair of duplex DNA. The spontaneous thermal disruption in base pairing at an A·T site may be sufficient to overcome the free energy barrier needed to partially bend DNA before forming a tight complex with IHF (*55*). Therefore, IHF (and possibly also HU) binding might be uncoupled from DNA bending. This could explain our results showing distinct Raman difference signatures for IHF:DNA in 100 and 250 mM NaCl. High salt (250 mM NaCl) may limit IHF-induced bending without greatly affecting IHF binding. This is consistent also with the observation that the T_m of the helix−coil transition in an oligonucleotide duplex increases with Na^+. Hence, an elevation in NaCl concentration that increases duplex stability may interfere with the ability of IHF to introduce a large static bend in the DNA target. Although we cannot exclude the possibility that high salt may also increase K_d by disrupting electrostatic interactions between IHF and the DNA target, the Raman results demonstrate a stable complex at the experimental conditions employed.

EMSA results show evidence of multiple protein/DNA complexes for both HUBst and IHF as the protein concentrations are increased above stoichiometric equivalency. For HUBst two additional complexes were observed, while for IHF only one additional complex was observed and only at a very high protein-to-DNA ratio (5:1). The latter complex, which is apparently unstable (gel smearing), may represent nonspecific binding of IHF to the stable 1:1 IHF:DNA complex. (The transient nature of the complex and the high concentration of protein required to produce it made further analysis by Raman spectroscopy impractical.) In the case of HUBst, Raman analysis of the 3:1 complex demonstrated that the structural reorganization of DNA in the complex is not simply the sum of two or more binding events. The perturbations are consistent with significant alterations in DNA base stacking, hydrogen bonding, bending, and unwinding. The data suggest a higher order arrangement of bound HUBst, possibly including higher order oligomers of the protein. The recruitment of additional HUBst molecules may be important in the normal cellular functioning of this protein. Such a result is consistent with the relatively high concentration of HU in the prokaryotic cell (30000 dimers per cell) (*56*). This result is also in accord with the proposal by Swinger and Rice that the flexibility of HU/DNA complexes may be biologically important by facilitating the formation of different higher order protein/DNA complexes (*6*). On the basis of the present results we speculate that if a modulation in bend angle occurs, it may involve the recruitment and binding of multiple HU molecules at a bending locus.

ACKNOWLEDGMENT

We thank Dr. Phoebe Rice, University of Chicago, for providing the plasmid containing the IHF insert and for many helpful suggestions during the course of this study.

REFERENCES

1. Arfin, S. M., Long, A. D., Ito, E. T., Tolleri, L., Riehle, M. M., Paegle, E. S., and Hatfield, G. W. (2000) Global gene expression profiling in *Escherichia coli* K12. The effects of integration host factor. *J. Biol. Chem. 275*, 29672–29684.
2. Paull, T. T., Haykinson, M. J., and Johnson, R. C. (1994) HU and functional analogs in eukaryotes promote Hin invertasome assembly. *Biochimie 76*, 992–1004.
3. Hwang, D. S., and Kornberg, A. (1992) Opening of the replication origin of *Escherichia coli* by DnaA protein with protein HU or IHF. *J. Biol. Chem. 267*, 23083–23086.
4. Polaczek, P., Kwan, K., Liberies, D. A., and Campbell, J. L. (1997) Role of architectural elements in combinatorial regulation of initiation of DNA replication in *Escherichia coli*. *Mol. Microbiol. 26*, 261–275.
5. Ryan, V. T., Grimwade, J. E., Nievera, C. J., and Leonard, A. C. (2002) IHF and HU stimulate assembly of pre-replication complexes at *Escherichia coli* oriC by two different mechanisms. *Mol. Microbiol. 46*, 113–124.
6. Swinger, K. K., and Rice, P. A. (2004) IHF and HU: flexible architects of bent DNA. *Curr. Opin. Struct. Biol. 14*, 28–35.
7. Rice, P. A., Yang, S.-W., Mizuuchi, K., and Nash, H. A. (1996) Crystal structure of an IHF-DNA complex: A protein-induced DNA U-turn. *Cell 87*, 1295–1306.
8. White, S. W., Appelt, K., Wilson, K. S., and Tanaka, I. (1989) A protein structural motif that bends DNA. *Proteins 5*, 281–288.
9. White, S. W., Wilson, K. S., Appelt, K., and Tanaka, I. (1999) The high-resolution structure of DNA-binding protein HU from *Bacillus stearothermophilus*. *Acta Crystallogr., Sect. D: Biol. Crystallogr. 55* (Part 4), 801–809.
10. Swinger, K. K., Lemberg, K. M., Zhang, Y., and Rice, P. A. (2003) Flexible DNA bending in HU-DNA cocrystal structures. *EMBO J. 22*, 3749–3760.
11. Christodoulou, E., Rypniewski, W. R., and Vorgias, C. R. (2003) High-resolution X-ray structure of the DNA-binding protein HU from the hyper-thermophilic *Thermotoga maritima* and the determinants of its thermostability. *Extremophiles 7*, 111–122.
12. Castaing, B., Zelwer, C., Laval, J., and Boiteux, S. (1995) HU protein of *Escherichia coli* binds specifically to DNA that contains single-strand breaks or gaps. *J. Biol. Chem. 270*, 10291–10296.
13. Kamashev, D., Balandina, A., and Rouviere-Yaniv, J. (1999) The binding motif recognized by HU on both nicked and cruciform DNA. *EMBO J. 18*, 5434–5444.
14. Pontiggia, A., Negri, A., Beltrame, M., and Bianchi, M. E. (1993) Protein HU binds specifically to kinked DNA. *Mol. Micrbiol. 7*, 343–350.
15. Kamashev, D., and Rouviere-Yaniv, J. (2000) The histone-like protein HU binds specifically to DNA recombination and repair intermediates. *EMBO J. 19*, 6527–6535.
16. Yang, S. W., and Nash, H. A. (1995) Comparison of protein binding to DNA *in vivo* and *in vitro*: defining an effective intracellular target. *EMBO J. 14*, 6292–6300.
17. Lorenz, M., Hillisch, A., Goodman, S. D., and Diekmann, S. (1999) Global structure similarities of intact and nicked DNA complexed with IHF measured in solution by fluorescence resonance energy transfer. *Nucleic Acids Res. 27*, 4619–4625.
18. Teter, B., Goodman, S. D., and Galas, D. J. (2000) DNA bending and twisting properties of integration host factor determined by DNA cyclization. *Plasmid 43*, 73–84.

19. Hodges-Garcia, Y., Hagerman, P. J., and Pettijohn, D. E. (1989) DNA ring closure mediated by protein HU. *J. Biol. Chem. 264*, 14621–14623.
20. Wojtuszewski, K., and Mukerji, I. (2003) HU binding to bent DNA: a fluorescence resonance energy transfer and anisotropy study. *Biochemistry 42*, 3096–3104.
21. Wojtuszewski, K., Hawkins, M. E., Cole, J. L., and Mukerji, I. (2001) HU binding to DNA: evidence for multiple complex formation and DNA bending. *Biochemistry 40*, 2588–2598.
22. Serban, D., Benevides, J. M., and Thomas, G. J., Jr. (2003) HU protein employs similar mechanisms of minor-groove recognition in binding to different *B*-DNA sites: demonstration by Raman spectroscopy. *Biochemistry 42*, 7390–7399.
23. Benevides, J. M., Serban, D., and Thomas, G. J., Jr. (2006) Structural perturbations induced in linear and circular DNA by the architectural protein HU from *Bacillus stearothermophilus*: Analysis by Raman spectroscopy. *Biochemistry 45*, 5359–5366.
24. Williams, L. D., and Maher, L. J., III (2000) Electrostatic mechanisms of DNA deformation. *Annu. Rev. Biophys. Biomol. Struct. 29*, 497–521.
25. Strauss-Soukup, J. K., Vaghefi, M. M., Hogrefe, R. I., and Maher, L. J., III (1997) Effects of neutralization pattern and stereochemistry on DNA bending by methylphosphonate substitutions. *Biochemistry 36*, 8692–8698.
26. Paolella, D. N., Liu, Y., Fabian, M. A., and Schepartz, A. (1997) Electrostatic mechanism for DNA bending by bZIP proteins. *Biochemistry 36*, 10033–10038.
27. Benevides, J. M., Chan, G., Lu, X. J., Olson, W. K., Weiss, M. A., and Thomas, G. J., Jr. (2000) Protein-directed DNA structure. I. Raman spectroscopy of a high- mobility-group box with application to human sex reversal. *Biochemistry 39*, 537–547.
28. Benevides, J. M., Li, T., Lu, X. J., Srinivasan, A. R., Olson, W. K., Weiss, M. A., and Thomas, G. J., Jr. (2000) Protein-directed DNA structure II. Raman spectroscopy of a leucine zipper bZIP complex. *Biochemistry 39*, 548–556.
29. Padas, P. M., Wilson, K. S., and Vorgias, C. E. (1992) The DNA-binding protein HU from mesophilic and thermophilic bacilli: gene cloning, overproduction and purification. *Gene 117*, 39–44.
30. Serban, D., Arcineigas, S. F., Vorgias, C. E., and Thomas, G. J., Jr. (2003) Structure and dynamics of the DNA-binding protein HU of *B. stearothermophilus* investigated by Raman and ultraviolet-resonance Raman spectroscopy. *Protein Sci. 12*, 861–870.
31. Welfle, H., Misselwitz, R., Welfle, K., Groch, N., and Heinemann, U. (1992) Salt-dependent and protein-concentration-dependent changes in the solution structure of the DNA-binding histone-like protein, HBsu, from *Bacillus subtilis*. *Eur. J. Biochem. 204*, 1049–1055.
32. Benevides, J. M., Wang, A. H. J., van der Marel, G. A., van Boom, J. H., Rich, A., and Thomas, G. J., Jr. (1984) The Raman spectra of left-handed DNA oligomers incorporating adenine-thymine base pairs. *Nucleic Acids Res. 12*, 5913–5925.
33. Benevides, J. M., Weiss, M. A., and Thomas, G. J., Jr. (1991) Design of the helix-turn-helix motif: nonlocal effects of quarternary structure in DNA recognition investigated by laser Raman spectroscopy. *Biochemistry 30*, 4381–4388.
34. Berjot, M., Marx, J., and Alix, A. J. P. (1987) Determination of the secondary structure of proteins from the Raman amide I band: the reference intensity profiles method. *J. Raman Spectrosc. 18*, 289–300.
35. Benevides, J. M., Wang, A. H. J., Rich, A., Kyogoku, Y., van der Marel, G. A., van Boom, J. H., and Thomas, G. J., Jr. (1986) Raman spectra of single crystals of r(GCG)d(CGC) and d(CCCCGGGG) as models for *A* DNA, their structure transitions in aqueous solution, and comparison with double-helical poly. (dG) ·poly. (dC). *Biochemistry 25*, 41–50.
36. Thomas, G. J., Jr., Benevides, J. M., Overman, S. A., Ueda, T., Ushizawa, K., Saitoh, M., and Tsuboi, M. (1995) Polarized Raman spectra of oriented fibers of *A*-DNA and *B*-DNA: anisotropic and isotropic local Raman tensors of base and backbone vibrations. *Biophys. J. 68*, 1073–1088.
37. Erfurth, S. C., Kiser, E. J., and Peticolas, W. L. (1972) Determination of the backbone structure of nucleic acids and nucleic acid oligomers by laser Raman scattering. *Proc. Natl. Acad. Sci. U.S.A. 69*, 938–941.
38. Erfurth, S. C., Bond, P. J., and Peticolas, W. L. (1975) Characterization of the *A*→*B* transition of DNA in fibers and gels by laser Raman spectroscopy. *Biopolymers 14*, 1245–1257.
39. Thomas, G. J., Jr., and Benevides, J. M. (1985) An *A*-helix structure for poly. (dA-dT)·poly. (dA-dT). *Biopolymers 24*, 1101–1105.
40. Benevides, J. M., and Thomas, G. J., Jr. (2005) Local conformational changes induced in *B*-DNA by ethidium intercalation. *Biochemistry 44*, 2993–2999.
41. Thomas, G. J., Jr., Benevides, J. M., and Prescott, B. (1986) DNA and RNA structures in crystals, fibers and solutions by Raman spectroscopy with applications to nucleoproteins, in *Biomolecular Stereodynamics* (Sarma, R. H., and Sarma, M. H., Eds.) pp 227–253, Adenine Press, Guilderland, NY.
42. Movileanu, L., Benevides, J. M., and Thomas, G. J., Jr. (2002) Temperature dependence of the Raman spectrum of DNA. II. Raman signatures of premelting and melting transitions of poly. (dA)·poly. (dT) and comparison with poly. (dA-dT)·poly. (dA-dT). *Biopolymers 63*, 181–194.
43. Nishimura, Y., Tsuboi, M., Sato, T., and Akoi, K. (1986) Conformation-sensitive Raman lines of mononucleotides and their use in a structure analysis of polynucleotides: guanine and cytosine nucleotides. *J. Mol. Struct. 146*, 123–153.
44. Peticolas, W. (1995) Raman spectroscopy of DNA and proteins. *Methods Enzymol. 246*, 389–417.
45. Toyama, A., Takeuchi, H., and Harada, H. (1991) Ultraviolet resonance Raman spectra of adenine, uracil and thymine derivatives in several solvents. Correlation between band frequencies and hydrogen-bonding states of the nucleic acid bases. *J. Mol. Struct. 242*, 87–98.
46. Benevides, J. M., Weiss, M. A., and Thomas, G. J., Jr. (1991) DNA recognition by the helix-turn-helix motif: Investigation by laser Raman spectroscopy of the phage lambda repressor and its interaction with operator sites OL1 and OR3. *Biochemistry 30*, 5955–5963.
47. Prescott, B., Steinmetz, W., and Thomas, G. J., Jr. (1984) Characterization of DNA secondary structure by Raman spectroscopy. *Biopolymers 23*, 235–256.
48. Benevides, J. M., and Thomas, G. J., Jr. (1983) Characterization of DNA structures by Raman spectroscopy: high-salt and low-salt forms of double helical poly. (dG-dC) in H_2O and D_2O solutions and application to *B*, *Z* and *A*-DNA. *Nucleic Acids Res. 11*, 5747–5761.
49. Movileanu, L., Benevides, J. M., and Thomas, G. J., Jr. (1999) Temperature dependence of the Raman spectrum of DNA. I. Raman signatures of premelting and melting transitions of poly. (dA-dT)·poly. (dA-dT). *J. Raman Spectrosc. 30*, 637–649.
50. Lu, X. J., Shakked, Z., and Olson, W. K. (2000) A-form conformational motifs in ligand-bound DNA structures. *J. Mol. Biol. 300*, 819–840.
51. Wojtuszewski, K., and Mukerji, I. (2004) The HU-DNA binding interaction probed with UV resonance Raman spectroscopy: structural elements of specificity. *Protein Sci. 13*, 2416–2428.
52. Broyles, S. S., and Pettijohn, D. E. (1986) Interaction of the *Escherichia coli* HU protein with DNA. Evidence for formation of nucleosome-like structures with altered DNA helical pitch. *J. Mol. Biol. 187*, 47–60.
53. Bonnefoy, E., and Rouviere-Yaniv, J. (1991) HU and IHF, two homologous histone-like proteins of *Escherichia coli*, form different protein-DNA complexes with short DNA fragments. *EMBO J. 10*, 687–696.
54. Sugimura, S., and Crothers, D. M. (2006) Stepwise binding and bending of DNA by *Escherichia coli* integration host factor. *Proc. Natl. Acad. Sci. U.S.A. 103*, 18510–18514.
55. Kuznetsov, S. V., Sugimura, S., Vivas, P., Crothers, D. M., and Ansari, A. (2006) Direct observation of DNA bending/unbending kinetics in complex with DNA-bending protein IHF. *Proc. Natl. Acad. Sci. U.S.A. 103*, 18515–18520.
56. Drlica, K., and Rouviere-Yaniv, J. (1987) Histonelike proteins of bacteria. *Microbiol. Rev. 51*, 301–319.
57. Overman, S. A., and Thomas, G. J., Jr. (1995) Raman spectroscopy of the filamentous virus *Ff (fd, f1, M13)*: Structural interpretation for coat protein aromatics. *Biochemistry 34*, 5440–5451.
58. Overman, S. A., and Thomas, G. J., Jr. (1999) Raman markers of nonaromatic side chains in an α-helix assembly: Ala, Asp, Glu, Gly, Ile, Leu, Lys, Ser, and Val residues of phage fd subunits. *Biochemistry 38*, 4018–4027.
59. Verduin, B. J., Prescott, B., and Thomas, G. J., Jr. (1984) RNA-protein interactions and secondary structures of cowpea chlorotic mottle virus for in vitro assembly. *Biochemistry 23*, 4301–4308.
60. Krafft, C., Benevides, J. M., and Thomas, G. J., Jr. (2002) Secondary structure polymorphism in *Oxytricha nova* telomeric DNA. *Nucleic Acids Res. 30*, 3981–3991.

BI7009426